ACS Catalysis

Perspective

Cite This: ACS Catal. 2019, 9, 1539−1548

pubs.acs.org/acscatalysis

What Is Measured When Measuring Acidity in Zeolites with Probe Molecules?

Mercedes Boronat* and Avelino Corma*

Instituto de Tecnología Química, Universitat Politècnica de València - Consejo Superior de Investigaciones Cientificas, Av. de los Naranjos, s/n, 46022 Valencia, Spain

ABSTRACT: Based on theoretical calculations of CO, NH_3, and pyridine adsorption at different sites in MOR and MFI zeolites, we analyze how confinement effects influence the measurement of acidity based on the interaction of probe molecules with Brönsted acid sites. Weak bases, such as CO, form neutral ZH−CO adducts with a linear configuration that can be distorted by spatial restrictions associated with the dimensions of the pore, leading to weaker interaction, but can also be stabilized by dispersion forces if a tighter fitting with the channel void is allowed. Strong bases such as NH_3 and pyridine are readily protonated on Brönsted acid sites, and the experimentally determined adsorption enthalpies include not only the thermochemistry associated with the proton transfer process itself, but also the stabilization of the $Z^-−BH^+$ ion pair formed upon protonation by multiple interactions with the surrounding framework oxygen atoms, leading in some cases to a heterogeneity of acidities within the same zeolite structure.

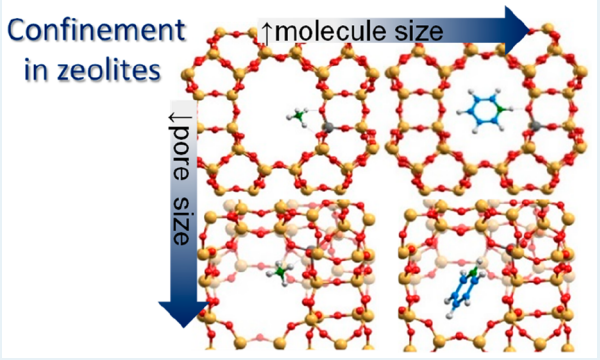

KEYWORDS: *Brönsted acid, confinement, DFT, dispersion, microporous structure*

Zeolites are inorganic microporous crystalline materials composed by SiO_4 and AlO_4 tetrahedra that link to form channels and cavities of molecular dimensions. Their well-determined topology and microporous structure, the associated high internal surface area, and their notable adsorption and shape-selective properties, are important aspects influencing their successful application as heterogeneous catalysts. Yet, the key factor in most catalytic applications is the presence of single, isolated, and well-defined active sites in the framework or in extra-framework positions which can be visualized, most of the time, by means of different physicochemical characterization techniques. Zeolites can be synthesized with a variety of pore dimensions and compositions. It is possible to introduce metal atoms in framework and extra-framework positions, as well as metal or metal oxide clusters within their channels and cavities. The substitution of tetrahedrally coordinated framework Si atoms with a trivalent element such as Al introduces bridging hydroxyl groups in the ordered structure of the solid. The presence of these bridging hydroxyl groups, with their Brönsted acid characteristics, have opened zeolites to a large number of academic and industrial applications, and it it possible to say that, today, zeolites are the most widely used solid acid catalysts in the industry.[1−8] They are employed in large-scale commercial processes in the fields of oil refining and the petrochemical industry, and they also find application in the production of fine and specialty chemicals, or in the conversion of methanol-to-olefins and methanol-to-gasoline (MTO and MTG processes, respectively). Moreover, their presence is increasing in emerging fields related with the nonconventional transformation of raw materials, such as the conversion of coal, gas, and oil into syngas, olefins, acetylene and aromatics, the potential transformation of alternative sources, such as biomass, and the valorization of methane or CO_2.[9−13]

Given that most industrial applications of zeolites are based on their Brönsted acid properties, it is not surprising that, since their introduction as acid catalysts,[14] a large effort has been done to characterize the number, strength, and accessibility of the potentially active acid sites, and to correlate these values with their catalytic activity. In addition to theoretical studies,[15−20] diverse experimental techniques such as calorimetric measurements, temperature-programmed desorption (TPD) of basic molecules, ^1H, ^{13}C, and ^{17}O solid-state nuclear magnetic resonance (NMR), as well as infrared (IR) and Raman vibrational spectroscopies, are employed to measure the acidity of zeolites.[21−30] Despite the accuracy of the theoretical and the experimental data obtained nowadays, and the deep understanding of zeolite acidity provided by such techniques, many questions are still open related to the heterogeneity of the Brönsted acid sites, either in different zeolites or within the same zeolite structure. This heterogeneity is associated with the location of the acid sites in pores, channels, and cavities of different dimensions, with the protons pointing to different environments, and should be taken into

Received: October 26, 2018
Revised: December 17, 2018
Published: January 8, 2019

DOI: 10.1021/acscatal.8b04317
ACS Catal. 2019, 9, 1539−1548

consideration when analyzing and comparing the acidity determined by different techniques.

By definition, a Brönsted acid is a species prone to donate a proton, according to

$$AH \rightarrow A^- + H^+$$

Or, in the presence of a base, a species able to transfer a proton to such base, as described by

$$AH + B \rightarrow A^- + BH^+$$

Following the first definition, the intrinsic strength of a Brönsted acid can be quantified by its deprotonation energy E_{DEP}, defined as the energy necessary to separate a proton at an infinite distance from the resulting anion,

$$E_{DEP} = E(A^-) + E(H^+) - E(AH)$$

However, in practice, Brönsted acidity can only be observed when a proton is transferred to a base, and, in this case, the feasibility of the process is also dependent on the tendency to accept protons, or proton affinity (PA), of the base,

$$PA = E(BH^+) - E(B) - E(H^+)$$

and of the stabilization of the resulting A^-−BH^+ ion pair by electrostatic and, depending on the system, other types of interactions. In solution, the ionic species A^- and BH^+ are fully surrounded by solvent molecules that provide a different degree of stabilization, depending on their polarity, and the dielectric medium decreases the Coulombic attraction between A^- and BH^+, facilitating their separation.[21,29]

In zeolites, the Brönsted acid sites are the so-called bridged hydroxyl groups (Figure 1), formed by a proton directly attached to a framework oxygen atom that is bonded to one Al and one Si atom. The three O−Al, O−Si, and O−H bonds are covalent bonds superimposed by small electrostatic interactions, and the O atom has therefore a formal 3-fold coordination similar to that present in the hydronium cation H_3O^+. The preferred geometry of an O atom in such nonclassical situation is not tetrahedral as in H_3O^+ cation, but has a tendency to be almost planar with three nonequivalent X−O−X bonds, where X = H, Al, and Si. The ordering imposed by the crystalline structure of the zeolite limits the flexibility around this O atom, thus weakening the OH bond and generating acidity. Deprotonation energies E_{DEP}, taken as the most rigorous parameter describing the intrinsic acid strength of a Brönsted acid, cannot be experimentally determined, but they have been estimated from quantum-chemical calculations using isolated clusters,[31,32] embedded clusters,[33−35] and periodic models.[18,36] Deprotonation energies calculated using small cluster models show important variations with cluster size that have a tendency to converge for systems containing more than 20 T atoms. This trend suggests that, at this cluster size, electrostatic interactions already approach those present in real zeolites.[32] Polarization of the Si−O bonds, which has been shown to be essential to stabilize the negative charge generated by deprotonation of the Brönsted acid centers, is also a quite local effect that does not extend far beyond the second O atom coordination sphere from the Al atom.[18] In accordance with this proposal and based on periodic DFT calculations, Grajciar et al. reported that the acidity of Brönsted sites in FER is mostly influenced by their local environment, in particular by the number of Al atoms in the second coordination sphere of the acid site, and not so much by the topology of the site.[36] This finding is especially relevant for zeolites with high Al content, and indirectly confirms the similar intrinsic acidity of all isolated Brönsted sites present in high Si/Al ratio zeolites. When the clusters treated with quantum chemical methods are embedded in a periodic system described by interatomic potentials, that is, the QM-Pot approach, the influence of cluster size is much smaller, and all calculated DPE values for FAU and MFI structures remain within 3 and 6 kJ/mol, respectively.[37] Deprotonation energy values calculated with the QM-Pot approach for various zeolites with different crystalline structure (CHA, TON, FER, MFI, MOR, and FAU) are within a range of <30 kJ/mol, indicating that the intrinsic acid strength of zeolites is hardly influenced by the framework structure.[34,37] This conclusion was confirmed by Jones et al. in an exhaustive and accurate study of deprotonation energies of isolated Brönsted acid sites in zeolites CHA, BEA, FER, MFI, MOR, and FAU. E_{DEP} for the 12 distinct T sites in MFI range from 1655 kJ/mol to 1668 kJ/mol, and from 1622 kJ/mol to 1665 kJ/mol in MOR (see all values in ref 18). The statistical ensemble averages of E_{DEP} values at each crystallographic position, which reflect the stability of the conjugate anions, are insensitive to the location of the isolated Al atoms, with calculated values of 1201 ± 11 kJ/mol.[18]

Therefore, the wide range of acid and catalytic properties reported for zeolite materials should be related to differences in the stabilization of the protonated BH^+ species by interaction with the negatively charged Z^- framework. The net negative charge in the deprotonated zeolite is easily spread out over the O atoms up to two coordination spheres from the Al center,[18] and provides a diffuse electron cloud over the inner surface of the zeolite microporous structure. This indicates that the zeolite anion would be a soft conjugated base, highly adaptable to stabilize soft cationic species confined within the pores.[38] The extent of this stabilization by electrostatic and van der Waals interactions is dependent on the number and strength of contacts between the confined species and the surrounding framework O atoms, that is, on how the size and shape of the

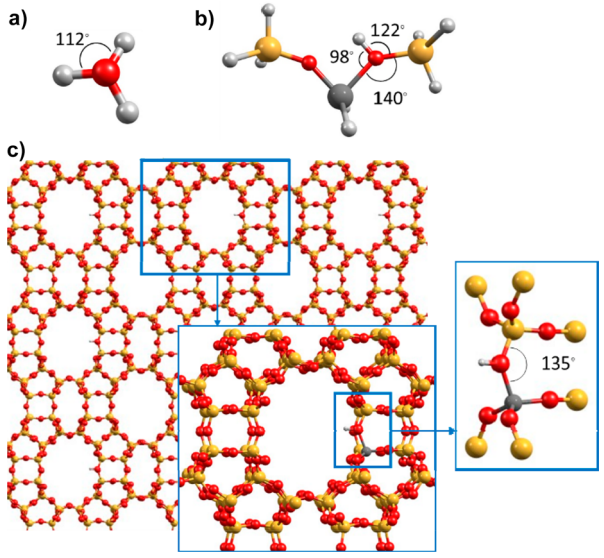

Figure 1. PBE/6-311g(d,p) optimized geometry of (a) H_3O^+ cation and (b) SiH_3−O−AlH_2−OH−$SiOH_3$ cluster. (c) Periodic model of a Brönsted acid site in MOR framework. [Legend: yellow balls, Si atoms; red balls, O atoms; gray balls, Al atoms; and white balls, H atoms.]

DOI: 10.1021/acscatal.8b04317
ACS Catal. 2019, 9, 1539−1548

guest species fits with those of the zeolite host channels and cavities.[19,39]

The confinement concept was introduced by Derouane et al., to rationalize some remarkable features of zeolites on the basis of the geometrical curvature of their internal surface.[40] In contrast to the shape-selectivity effects, which modify the adsorption and diffusion of reactants and products, or prevents the formation of certain transition states, because of short-range repulsions between the adsorbed molecules and the zeolite microporous structure, confinement effects stem from long-range attractive van der Waals interactions. When the sizes of the host structure and the guest molecule become comparable, the adsorbed molecules and their direct framework environment have a tendency to reciprocally optimize their van der Waals interaction, leading to enhanced adsorption, diffusion, and catalytic properties.[41] A first and simple model to quantify van der Waals interactions in confined spaces considered dispersion forces only, and was based on a dimensionless parameter s, which was defined as

$$s = \frac{d}{a}$$

where d is the distance between the confined molecule and the micropore wall and a is the micropore radius. The magnification of dispersion interactions in a curved environment, relative to a flat surface, was estimated as being proportional to $(1 - s/2)^{-3}$, and suggested that physisorption energies could be enhanced by a factor of 8 in the situation of maximum confinement ($s = 1$), and by a factor of ∼3 in intermediate situations ($0.5 < s < 1$). Further improvement of this model by including pore shape and repulsion effects led to a maximum magnification of the physisorption energy by a factor of ∼5 in the optimal tight fit situation.[40,41]

Many efforts have been done since then to quantitatively evaluate confinement effects in zeolites, considering not only the average size of molecules and channels, but also molecular shape and local framework geometry within the pores. Methods based on classical force fields have been widely used to simulate molecular adsorption and diffusion in zeolites, because of their computational efficiency and accuracy.[42] However, they are not suited to describe chemical reactions involving bond breaking and formation, and, therefore, quantum mechanical (QM) methods, despite being computationally more expensive, have been applied to the study of reactivity in zeolites. QM methods are applied to cluster models in which a portion of the zeolite is taken into account, to hybrid schemes combining clusters treated at QM level inserted in a periodic system described with force fields, or to fully periodic systems.[15,16,19] In the case of periodic calculations based on density functional theory (DFT), one of the main challenges is the description of the dispersion interactions, which are not taken into consideration by local density functionals. Several approaches have emerged in recent years to overcome this limitation, and encouraging results have been reported, for instance, for the adsorption of alkanes in zeolites using computationally accessible techniques.[43−45] Among them, the DFT-D methodology proposed by Grimme combines an excellent computational efficiency with reasonable accuracy, with an average deviation from experimental values of ∼5 kJ/mol.[46,47]

To illustrate the effect of confinement associated with the curvature of the zeolite microporous structure, four molecules of increasing size and polarity—CO, CH_4, NH_3, and pyridine—have been placed within the channels of pure siliceous models of mordenite (MOR) and ZSM-5 (MFI), and their position optimized without restrictions at the DFT level (see Figures 2 and 3). The channel system of MFI is composed

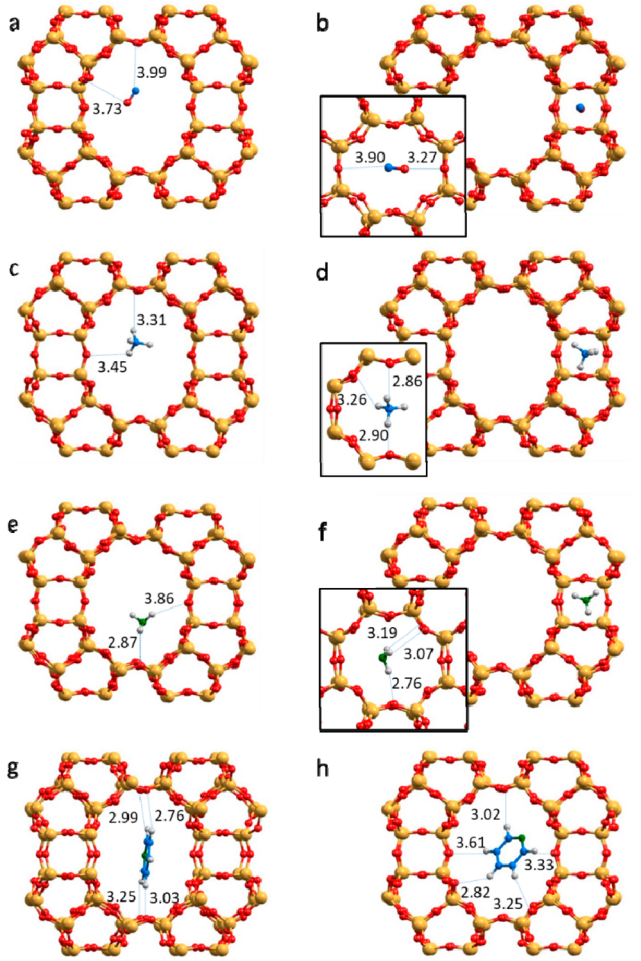

Figure 2. Optimized structures of (a, b) CO, (c, d) CH_4, (e, f) NH_3, and (g, h) pyridine placed in the main channel and side-pockets of a pure siliceous model of MOR zeolite.

by interconnected straight and sinusoidal 10-ring (10R) channels ∼5.0 Å in diameter, that intersect, forming larger void spaces ∼7.0 Å in diameter, while MOR contains large 12R channels of ∼7.0 Å interconnected via small 8R side pockets of ∼4.0 Å. Two initial positions were considered for each molecule in each zeolite: in the 12R channels and 8R side pockets in MOR, and in the 10R channels and at the channel intersections in MFI.

The main contribution to the calculated interaction energies corresponds to dispersion forces (E_{int} D3 in Table 1), in agreement with previous work.[44] In general, along the series of guest molecules and host zeolites, this term becomes larger as the size of the molecule increases, CO < NH_3 ≈ CH_4 < Py, and as the diameter of the channel decreases, MOR-12R < MFI-int < MFI-10R < MOR-8R, with the calculated values ranging from −20 kJ/mol to −70 kJ/mol. Only for NH_3 in the side-pockets of MOR, the presence of some local hydrogen bonding between the slightly positive H atoms and three close O atoms in the ring, results in a comparable contribution of the pure DFT and the D3 values to the calculated interaction energy.

DOI: 10.1021/acscatal.8b04317
ACS Catal. 2019, 9, 1539−1548

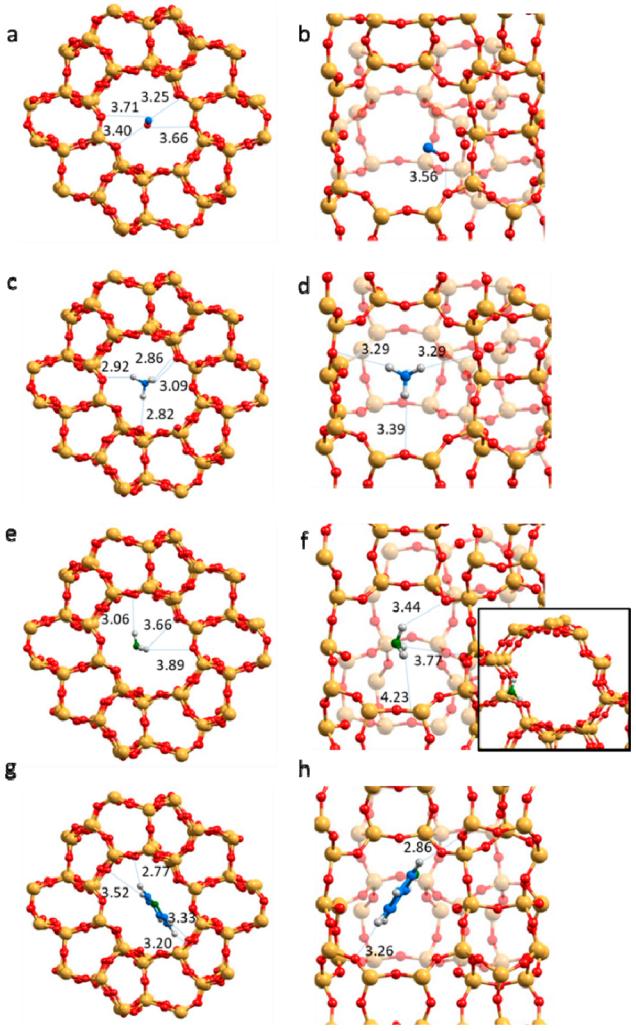

Figure 3. Optimized structures of (a, b) CO, (c, d) CH_4, (e, f) NH_3, and (g, h) pyridine placed in the 10R channel and at the channels intersection of a pure siliceous model of MFI zeolite.

The orientation of Py within the 12R channels of MOR results in a non-negligible difference in dispersion effects of 6 kJ/mol favoring the perpendicular orientation. In the narrower channels of MFI, however, Py moves slightly toward the wider region at the intersection, so that the global confinement in the two positions initially considered is similar, and larger than in MOR. These stabilizing interactions, associated only to confinement in curved environments, have been generally taken into consideration to study adsorption of hydrocarbons in zeolites,[48] and, more recently, have been included in reactivity studies.[39] We analyze now how these confinement effects influence the measurements of acidity based on interaction of probe molecules with Brönsted acid sites.

The adsorption of probe molecules of weak basicity such as N_2, CO, ethene, propane, CH_3CN, or methanol, and the measurement of the perturbation of the ν(OH) frequency by formation of a ZH−B adduct between the Brönsted acid site and the weak base, have been widely used to quantify acid strength in zeolites.[21,25,28] Upon formation of a weak hydrogen bond with a base such as CO, the ν(OH) stretching frequency of different zeolites undergoes a red shift of up to 400 cm^{-1}, while the ν(CO) vibrational frequency is blue-shifted by 30−40 cm^{-1}, with the magnitude of the shifts being assumed to be proportional to the acidity of the OH group and, therefore, to the strength of the interaction.[24,49,50]

Table 1. Interaction Energies Calculated for CO, CH_4, NH_3, and Py within the Channels System of Pure Silica Mordenite

		Interaction Energy (kJ/mol)		
molecule	position	E_{int} PBE	E_{int} D3	E_{int} PBE-D3
CO	MOR-12R	−13	−8	−21
CO	MOR-8R	−13	−25	−38
CO	MFI-int	−1	−19	−20
CO	MFI-10R	−1	−24	−25
CH_4	MOR-12R	−13	−11	−24
CH_4	MOR-8R	−11	−30	−41
CH_4	MFI-int	−2	−22	−24
CH_4	MFI-10R	1	−29	−28
NH_3	MOR-12R	−4	−16	−19
NH_3	MOR-8R	−26	−25	−52
NH_3	MFI-int	−6	−18	−24
NH_3	MFI-10R	−9	−25	−34
Py	MOR-12R ∥	−17	−49	−67
Py	MOR-12R ⊥	−21	−54	−75
Py	MFI-int	−6	−70	−76
Py	MFI-10R	−3	−69	−72

Indeed, accurate measurements of enthalpy changes associated with CO bonding to Brönsted acid sites in H−Y, H-ZSM-5, and H-FER zeolites were found to correlate with the shift in the ν(OH) frequency. However, the trend did not apply for H-MCM-22 and H-MCM-56 zeolites.[51] Using surface science techniques in a UHV environment, Boscoboinik et al. characterized the acidity of a bidimensional zeolite model system consisting of a bilayer aluminosilicate film supported on Ru(0001) surface. The red-shift in the ν(OH) frequency induced by CO and ethene adsorption on the bridged hydroxyl groups present in the 2D model was in the order of the most acidic OH groups reported for zeolites, indicating that the aluminosilicate film is more acidic than 3D zeolites. However, the calculated adsorption energies were larger in the zeolite cavities than in the flat surface, because of the larger contribution of dispersion interactions in the curved surfaces of 3D zeolites.[52,53] Therefore, it seems that a number of factors can influence the measured shifts apart from the intrinsic acidity of the Brönsted site, at least some of them being associated with the confinement effect. In order to gain a deeper insight into how the confinement effect associated with micropores of different diameter affects the characterization of acidity by means of CO adsorption, the interaction of CO with 10 Brönsted acid sites located in the 12R channels and 8R pockets of MOR, and in the 10R channels and channels intersections of MFI, with the protons pointing to different environments, has been investigated using the DFT-D3 approach.

There are four nonequivalent tetrahedral sites in the MOR unit cell, T1 in the 12R main channel, T2 and T4 at the intersection between the 12R channel and the 8R side-pockets, and T3 inside the 8R pockets. To cover different environments of the acid centers, an Al atom was introduced at T1, T3, and T4 positions and, in each case, two different Brönsted acid sites were generated by attaching a proton to two out of the four different O atoms directly bonded to Al, labeled O_a and O_b

DOI: 10.1021/acscatal.8b04317
ACS Catal. 2019, 9, 1539−1548

(Figure 4). Among the 12 nonequivalent tetrahedral sites present in the orthorhombic structure of MFI, T4 and T10 are

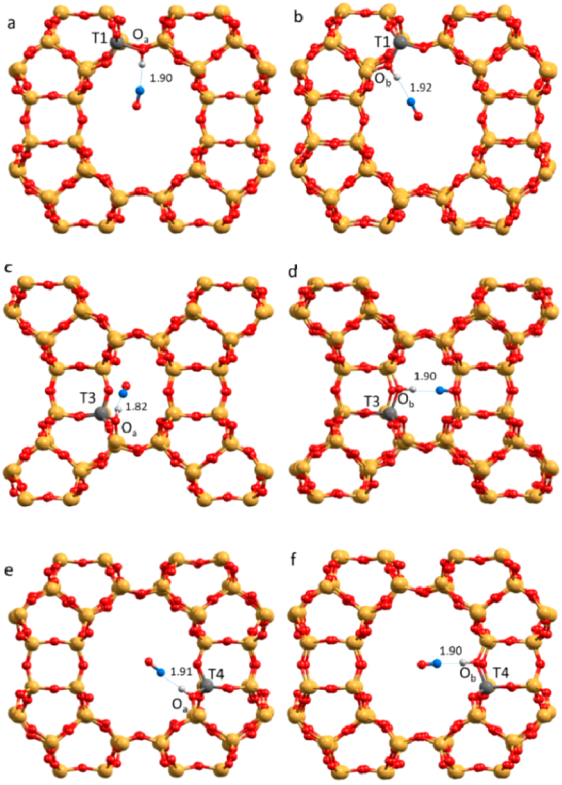

Figure 4. Optimized structures of CO interacting with Brönsted acid sites placed in the (a, b, e, f) main channel and (c, d) side pockets of MOR zeolite.

located in the sinusoidal 10R channel, T8 and T11 are in the straight 10R channel, and the rest (T1, T2, T3, T5, T6, T7, T9, and T12) are at the intersection between the sinusoidal and straight 10R channels. We studied two different environments, one within the straight 10R channels by placing an Al at T11 site, and another one at the wider void at the channels intersection with Al located at T1. And again, in each case, two possible orientations of the Brönsted acid site were considered, depending on the oxygen atom, O_a or O_b, to which the proton was attached (Figure 5). Interaction energies with and without dispersion corrections are summarized in Table 2, together with the shifts in the νOH vibrational frequencies obtained using the accurate ω/r correlation method described by Nachtigall et al.[54]

The optimized geometry of the adducts formed by interaction of CO with a Brönsted acid site is linear, with optimized ZH−CO distances close to ∼2 Å, and with the CO molecule occupying the void space to which the proton in the isolated site was pointing. However, if the dimensions of the pore do not allow a linear configuration or there are spatial restrictions forcing a hydrogen bond that is too short/too long, the acid−base interaction is weaker and the system is slightly destabilized. On the other hand, depending on the architecture of the microporous system, some configurations allow a tighter fitting of CO within the channel void, leading to a larger stabilization by dispersion interactions. Both effects are independent and can contribute to the final geometry and stability of the system.

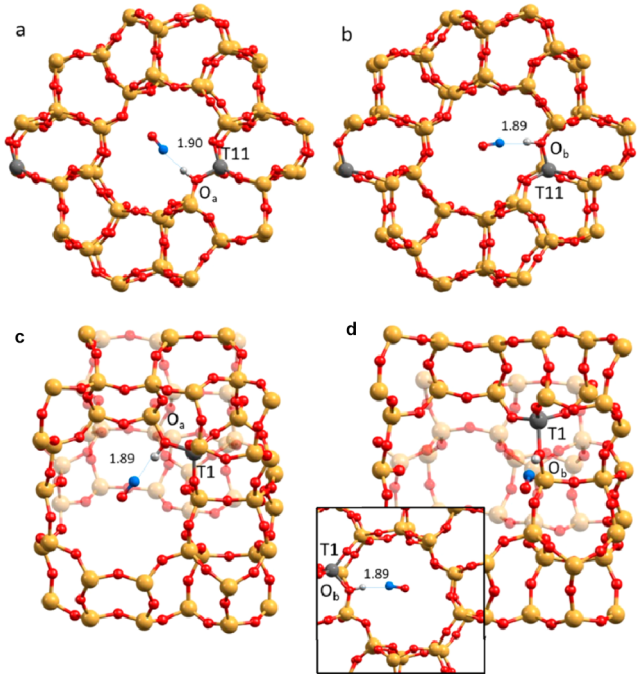

Figure 5. Optimized structures of CO interacting with Brönsted acid sites placed (a, b) in the 10R channel and (c, d) at the channels intersection of MFI zeolite.

This is clearly observed, for example, when comparing the adsorption of CO at T3 and T4 sites in MOR. The geometry of the adduct formed at T3−O_a site should be equivalent to that obtained at T4−O_a site (Figures 4c and 4e), but the proximity of other framework oxygen atoms belonging to the narrow sinusoidal 8R channel restricts the free space available for CO, so that the optimized H−CO distance, 1.82 Å, is the shortest among all the computed values, and the DFT interaction energy is 10 kJ/mol lower than observed at T4−O_a. The local geometry of the adducts formed at T3−O_b and T4−O_b sites in MOR seems similar (Figures 4d and 4f) but CO adsorption at T3−O_b provokes a distortion of the dihedral angle d(H−O−Al−O) from 13° to 69°, which results in a low interaction energy at the DFT level, while on T4−O_b the d(H−O−Al−O) dihedral angle only changes from 11° to 29°, because of the interaction with CO. Counteracting this effect, we observe that, while in T3−O_a and T3−O_b, the CO molecule is closely surrounded by the O atoms of the 8R, in T4−O_a and T4−O_b, it is placed at the center of the large 12R channel, which results in differences in stabilization by dispersion forces of nearly 20 kJ/mol (Table 2). Altogether, the total adsorption energies are larger at T3 than at T4, which correlates with larger $\Delta\nu$(OH) frequency shifts at T3. However, this trend is lost when T1 is included in the comparison. The largest total interaction energy in MOR is obtained for T1−O_b site with CO crossing the main 12R channel, but the calculated $\Delta\nu$(OH) shift in this position is the lowest, −278 cm^{-1}. In contrast, for the environments considered within MFI structure, both the Brönsted sites associated with Al atoms placed at the 10R channels and those placed at the channels intersections are able to form ZH−CO adducts with the proton and CO oriented toward the void space at the intersections (Figure 5), without any geometrical constraint associated with the presence of too close framework atoms. The differences in the DFT and D3 contributions

DOI: 10.1021/acscatal.8b04317
ACS Catal. 2019, 9, 1539−1548

Table 2. Interaction of CO with Brönsted Acid Sites in MOR and MFI

				Interaction Energy (kJ/mol)			
zeolite	site	location	r(H−CO) (Å)	E_{int} DFT	E_{int} D3	E_{int} DFT-D3	$\Delta\nu$(OH) (cm^{-1})
MOR	T1-O_a	12R	1.897	−25	−18	−43	−368
MOR	T1-O_b	12R	1.915	−38	−16	−53	−278
MOR	T3-O_a	8R	1.819	−17	−35	−52	−426
MOR	T3-O_b	8R	1.896	−14	−33	−47	−419
MOR	T4-O_a	8R	1.911	−27	−16	−42	−346
MOR	T4-O_b	12R	1.901	−24	−15	−39	−345
MFI	T1-O_a	int	1.891	−25	−24	−49	−366
MFI	T1-O_b	int	1.893	−24	−26	−50	−378
MFI	T11-O_a	10R	1.905	−33	−17	−50	−357
MFI	T11-O_b	10R	1.895	−33	−16	−49	−358

between sites are lower than 10 kJ/mol, the total interaction energies are within 1 kJ/mol, and the shifts in the ν(OH) vibrational frequencies are in a narrow range of 20 cm^{-1}.

These results show that there are several independent factors contributing to the optimized geometry, ν(OH) frequency, and stability of ZH−CO adsorption complexes, which explain the lack of correlation between CO adsorption energies and induced $\Delta\nu$(OH) shifts in some cases,[51,53] and questions the use of these shifts to evaluate the acid strength of zeolites and its influence on reactivity.

In contrast to weak bases such as CO, strong bases such as NH_3 and pyridine are protonated by Brönsted acid sites, and the resulting cationic species, NH_4^+ and pyridinium$^+$ cations, interact strongly with the negatively charged zeolite framework. Temperature-programmed desorption (TPD) of NH_3, Py, and other amines with different degrees of substitution, is one of the most widely used methods for quantifying Brönsted acidity in zeolites.[1,21,29,55−57] It is based on an initial saturation of the catalyst surface with chemisorbed NH_3 or amine followed by a linear increase in the temperature, with the amount of NH_3 or amine desorbed at different temperatures providing information about the concentration and strength of the acid sites present. Adsorption enthalpies obtained from TPD measurements include not only the thermochemistry associated with the proton transfer process itself, but also the stabilization of the Z^-BH^+ ion pair formed upon protonation by multiple interactions with the surrounding framework oxygen atoms. A simple thermochemical cycle was proposed by Gorte and collaborators to understand the acidity of zeolites, as depicted in Figure 6.[29,55,58,59]

According to this scheme, the experimentally measured heat of adsorption ($\Delta H_{adsorption}$) of a strong base B in a zeolite ZH includes the deprotonation energy of the zeolite (E_{DEP}), the proton affinity of the base (PA_B), and the specific stabilization of the Z^-BH^+ ion pair within the zeolite void where it is formed ($\Delta H_{interaction}$), or, in other words, the confinement effect of a particular zeolite on a given molecule. Since the deprotonation energies of all sites in all zeolites are similar,[18,34,37] the measured adsorption enthalpies for one base in different zeolites are indicative of the different confinement effects exerted by these zeolites on this base. Thus, for instance, the larger experimental enthalpies of adsorption of NH_3 in H-MOR (160 kJ/mol), compared to H-ZSM-5 (145 kJ/mol), indicate a larger ion-pair stabilization or confinement effect in the voids of mordenite.[59] On the other hand, the existence of a correlation between the heats of adsorption and the proton affinities of a series of alkyl amines in H-MOR and H-ZSM-5 (Figure 6b) suggests that confinement effects within a given zeolite structure are similar, in principle, for a series of structurally related bases. The negative deviation from the correlation found for trimethylamine was attributed to the loss of one hydrogen bond with the framework in $(CH_3)_3NH^+$ cation, compared to NH_4^+ or the other protonated primary or secondary amines, while the higher-than-expected adsorption enthalpies obtained for butylamine were explained on the basis of an enhanced stabilization by dispersion interactions between the alkyl chain and the pore walls.[59] While these and similar results reported for substituted pyridines provide a clear picture of the role of confinement in stabilizing protonated bases in different zeolite structures, they do not reflect the possibility of having a heterogeneous distribution of Brönsted acid sites within a particular zeolite associated with their location in voids of different size. To add some information regarding this possibility, we have now calculated the energetics of adsorption and protonation of NH_3 and pyridine at different sites in MOR and MFI structures, so

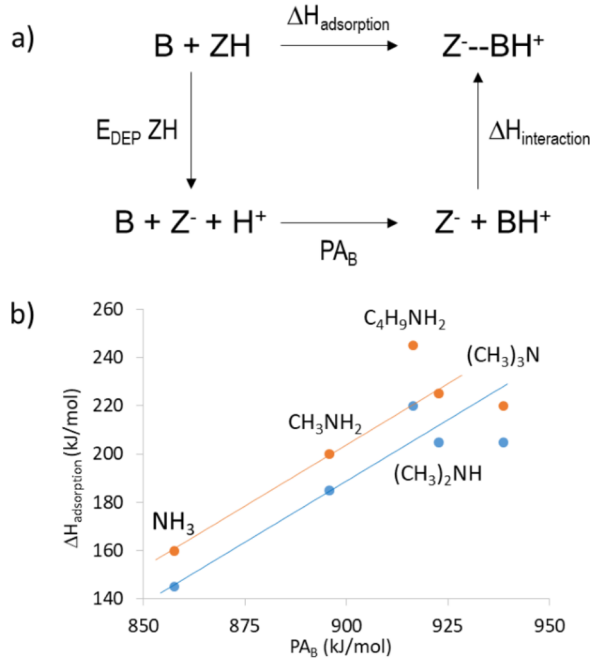

Figure 6. Thermochemical cycle for (a) acidity in zeolites and (b) correlation between heats of adsorption ($\Delta H_{adsorption}$) and proton affinities (PA) of alkylamines in H-MOR (orange) and H-ZSM-5 (blue). [Adapted from ref 59. Copyright 1996, American Chemical Society, Washington, DC.]

DOI: 10.1021/acscatal.8b04317
ACS Catal. 2019, 9, 1539−1548

that the role of confinement in different regions of the same zeolite can be estimated and compared.

All Brönsted acid sites in MOR and MFI structures are accessible to NH_3, which, upon interaction with a bridged hydroxyl group, is spontaneously protonated, forming a Z^-–NH_4^+ ion pair. The interaction energies calculated for the process Z–H + NH_3 → Z^-–NH_4^+ at a pure DFT level are significantly higher than those obtained for CO adsorption, reflecting the much stronger interaction between charged species, while the contribution of dispersion interactions included in the D3 term is, in this case, less relevant. In all cases, NH_4^+ remains close to the Al atom, forming two strong hydrogen bonds with the two most accessible oxygen atoms directly attached to Al. The optimized H--O distances in the ion-pair complexes in which NH_4^+ is occupying the free space in the straight 12R of MOR or 10R channels in MFI are quite similar (∼1.65 and ∼1.71 Å; see Figures 7a, 7c, and 7e).

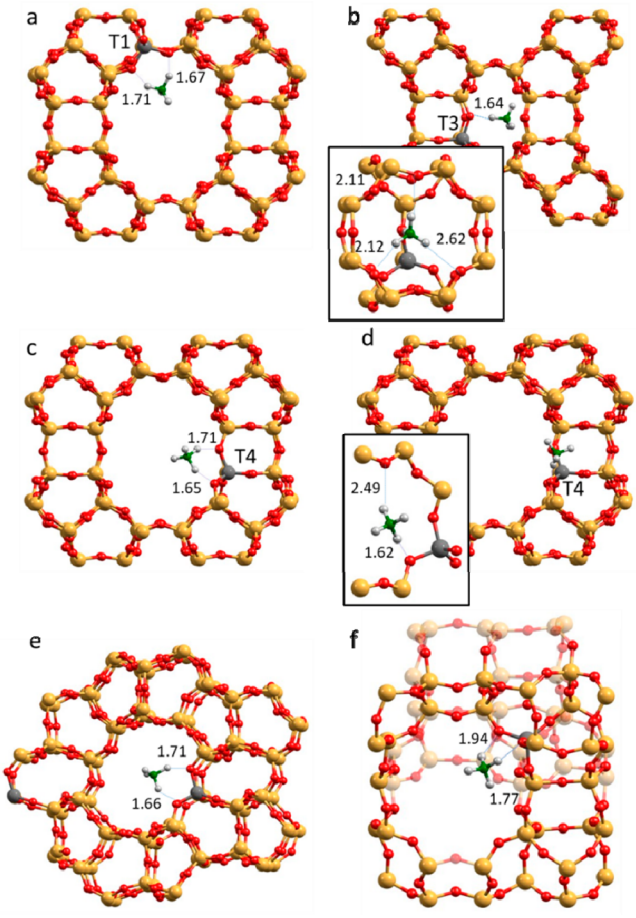

Figure 7. Optimized structures of NH_3 protonated by Brönsted acid sites placed in (a, c) the main channel and (b, d) in the side pockets of MOR, and (e) in the straight channel and (f) the channels intersection of MFI zeolites.

However, the presence of other close O atoms in the pockets of MOR or at the channels intersection in MFI readily distort this geometry. Thus, when NH_3 is protonated at T3 inside the MOR pockets, the NH_4^+ cation is stabilized by one short bond with the oxygen attached to Al and by three weaker hydrogen bonds with the framework O atoms of the 8R (Figure 7b). Moreover, the contribution of dispersion forces in this position is larger than in the main channel, and, altogether, the calculated interaction energy at T3 is the largest of all values in Table 3. A similar conformation was explored at T4, with NH_3 initially placed within the 8R; however, in this case, only one extra hydrogen bond was formed to stabilize NH_4^+ (Figure 7d). Finally, the relative orientation of the four oxygen atoms directly bonded to Al in the T1 site in MFI (Figure 7e) does not allow the formation of a clear bidentate complex, and, consequently, the adsorption energy of NH_3 at the channels intersection in MFI is 20 kJ/mol weaker than within the channels. The average of the calculated values for NH_3 chemisorption in MFI are in very good agreement with the experimental data obtained by Lee et al. (145 kJ/mol),[59] who also reported a higher value for the adsorption energy of NH_3 in MOR, 160 kJ/mol. In this case, the measured data agrees with the adsorption energy calculated at the most stable site in MOR, inside the 8R pockets, but does not reflect the heterogeneity of sites in MOR regarding the stabilization of the Z^-–NH_4^+ ion-pair.

Table 3. Interaction of NH_3 and Pyridine with Brönsted Acid Sites Placed in the Main Channels and Side Pockets of MOR and in the 10R Channels and Channels Intersections of MFI

			Interaction Energies (kJ/mol)		
molecule	site	location	E_{int} DFT	E_{int} D3	E_{int} DFT-D3
NH_3	MOR-T1	12R	−127	−20	−148
NH_3	MOR-T3	8R	−135	−34	−169
NH_3	MOR-T4a	12R	−124	−16	−140
NH_3	MOR-T4b	8R	−124	−27	−151
NH_3	MFI-T1	int	−114	−21	−135
NH_3	MFI-T11	10R	−138	−17	−155
pyridine	MOR-T1	12R	−147	−63	−210
pyridine	MOR-T4a	12R	−143	−62	−205
pyridine	MFI-T1	int	−142	−69	−211
pyridine	MFI-T11	10R	−154	−68	−222

The protonation of pyridine, according to Z–H + Py → Z^-–Py^+ generates a planar pyridinium cation that can only form monodentate adducts with one of the O atoms directly bonded to Al and that, because of the different size and bonding geometry, compared to NH_3, has a tendency to occupy, in all cases, the void spaces in the large 12R channels in MOR or at the channels intersections in MFI (Figure 8). Thus, while neutral Py adsorbed parallel to the channels axis in pure siliceous models of MOR and MFI (Figures 2 and 3), once it is protonated, stronger hydrogen bonds between the five H atoms attached to C and framework oxygen atoms are formed, which change the orientation of the molecule to maximize such hydrogen bond interactions. As a consequence, only adducts with a Py^+ cation perpendicular to the 12R channel axis in MOR and occupying the space at the channels intersections in MFI are obtained. In this situation, both the electrostatic interactions correctly reproduced at the DFT level and the dispersion contributions included in the D3 term are comparable in all adducts (Table 3). The total interaction energies are independent of the zeolite framework and location of Al, and are in excellent agreement with the experimental values reported for pyridine adsorption in H-ZSM-5 and H-MOR, 200 kJ/mol.[59]

In summary, while it is accepted today that the intrinsic acidity of bridged hydroxyl groups in high Si/Al ratio zeolites

DOI: 10.1021/acscatal.8b04317
ACS Catal. 2019, 9, 1539−1548

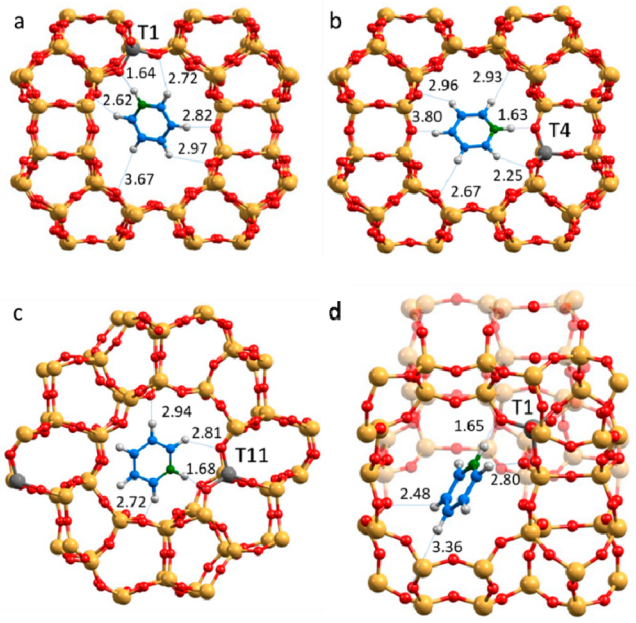

Figure 8. Optimized structures of Pyridinium cation formed by protonation of pyridine by Brönsted acid sites placed in the main channel of (a, b) MOR and in the (c) straight channel and (d) channels intersection of MFI zeolites,.

determined by their deprotonation energy is independent of zeolite structure or site location within the framework, a more complex situation is found when acidity is measured by means of adsorption of probe molecules. Weak bases interacting with Brönsted acid sites form neutral ZH−B adducts whose preferred geometry can be distorted by spatial restrictions associated with the pore dimensions and to the relative orientation of the adduct within the microporous structure. On the other hand, and depending on the location of the Brönsted acid sites within the microporous system, i.e. in channels, cavities or pockets, a larger stabilization by dispersion forces can be obtained when there is a tight fitting of the probe molecule with the confining void. Strong bases interacting with Brönsted acid sites become protonated, and the adsorption enthalpies obtained with calorimetric or TPD techniques go beyond the thermochemistry of the proton transfer process and, therefore, beyond the measurement of "acidity", because they also include the stabilization of the Z^-−BH^+ ion pair formed upon protonation by multiple interactions with the surrounding framework O atoms. Therefore, unless all these factors are uncoupled, the conventional methods based on adsorption of probe molecules cannot determine the intrinsic acidity of the acid sites of zeolites. Nevertheless, since different probe molecules form adducts whose size, geometry, and location within the confining voids results in different destabilizing constraints and stabilizing dispersion interactions, the use of series of probe molecules can still be informative. Indeed, by combining theoretical results as exemplified here with adequate adsorption experiments, it should be possible, with a structurally known zeolite, to determine the degree of heterogeneity of the acid sites present, depending on the synthesis or post-synthesis conditions. Finally, if the zeolite is to be applied in a particular reaction, the combination of the theoretical work outlined before with adsorption and kinetic studies should give information about the acid sites interacting, their geometries and energetic implications, and where to locate the acid sites within the zeolite structure to maximize activity and selectivity.

COMPUTATIONAL DETAILS

All calculations are based on periodic density functional theory (DFT) and were performed using the Perdew−Burke−Ernzerhof (PBE) exchange-correlation functional within the generalized gradient approach (GGA),[60,61] as implemented in the Vienna Ab-initio Simulation Package (VASP) code.[62] The valence density was expanded in a plane wave basis set with a kinetic energy cutoff of 500 eV, and the effect of the core electrons in the valence density was taken into account by means of the projected augmented wave (PAW) formalism.[63] Integration in the reciprocal space was carried out at the Γ *k*-point of the Brillouin zone. During geometry minimizations, the positions of all atoms in the systems were fully relaxed without any restriction. Dispersion corrections to the energies were evaluated using the D3 Grimme's method.[46,47]

AUTHOR INFORMATION

Corresponding Authors

*E-mail: boronat@itq.upv.es (M. Boronat).
*E-mail: acorma@itq.upv.es (A. Corma).

ORCID

Mercedes Boronat: 0000-0002-6211-5888
Avelino Corma: 0000-0002-2232-3527

Notes

The authors declare no competing financial interest.

ACKNOWLEDGMENTS

This work was supported by the European Union through No. ERC-AdG-2014-671093 (SynCatMatch), and by the Spanish Government-MINECO through "Severo Ochoa" (No. SEV-2016-0683) and No. MAT2017-82288-C2-1-P projects. Red Española de Supercomputación (RES) and Centre de Càlcul de la Universitat de València are gratefully acknowledged for computational resources.

REFERENCES

(1) Chen, H.-Y. In *Urea−SCR Technology for deNOx After Treatment of Diesel Exhausts*; Nova, I., Tronconi, E., Eds.; Springer: New York, 2014; pp 123−147. Corma, A. Inorganic Solid Acids and Their Use in Acid-Catalyzed Hydrocarbon Reactions. *Chem. Rev.* **1995**, *95*, 559−614.
(2) Corma, A. From Microporous to Mesoporous Molecular Sieve Materials and Their Use in Catalysis. *Chem. Rev.* **1997**, *97*, 2373−2419.
(3) Clerici, M. G. Zeolites for Fine Chemicals Production. *Top. Catal.* **2000**, *13*, 373−386.
(4) Haw, J. F.; Song, W. G.; Marcus, D. M.; Nicholas, J. B. The Mechanism of Methanol to Hydrocarbon Catalysis. *Acc. Chem. Res.* **2003**, *36*, 317−326.
(5) Corma, A. State of the Art and Future Challenges of Zeolites as Catalysts. *J. Catal.* **2003**, *216*, 298−312.
(6) Bhan, A.; Iglesia, E. Link between Reactivity and Local Structure in Acid Catalysis on Zeolites. *Acc. Chem. Res.* **2008**, *41*, 559−567.
(7) Wang, W.; Hunger, M. Reactivity of Surface Alkoxy Species on Acidic Zeolite Catalysts. *Acc. Chem. Res.* **2008**, *41*, 895−904.
(8) Martínez, C.; Corma, A. Inorganic Molecular Sieves: Preparation, Modification and Industrial Application in Catalytic Processes. *Coord. Chem. Rev.* **2011**, *255*, 1558−1580.
(9) Vermeiren, W.; Gilson, J.-P. Impact of Zeolites on the Petroleum and Petrochemical Industry. *Top. Catal.* **2009**, *52*, 1131−1161.

DOI: 10.1021/acscatal.8b04317
ACS Catal. 2019, 9, 1539−1548

(10) Yilmaz, B.; Müller, U. Catalytic Applications of Zeolites in Chemical Industry. *Top. Catal.* **2009**, *52*, 888−895.
(11) Rinaldi, R.; Schuth, F. Design of Solid Catalysts for the Conversion of Biomass. *Energy Environ. Sci.* **2009**, *2*, 610−626.
(12) Olsbye, U.; Svelle, S.; Lillerud, K. P.; Wei, Z. H.; Chen, Y. Y.; Li, J. F.; Wang, J. G.; Fan, W. B. The Formation and Degradation of Active Species during Methanol Conversion over Protonated Zeotype Catalysts. *Chem. Soc. Rev.* **2015**, *44*, 7155−7176.
(13) Abate, S.; Barbera, K.; Centi, G.; Lanzafame, P.; Perathoner, S. Disruptive Catalysis by Zeolites. *Catal. Sci. Technol.* **2016**, *6*, 2485−2501.
(14) Rabo, J. Gajda, G. J. In *Guidelines for Mastering the Properties of Molecular Sieves*; Barthomeuf, D., Derouane, E. G., Hoelderich, W., Eds.; NATO ASI, Series B: Physics, Vol. *221*; Plenum Press: New York, 1990; p 273.
(15) Sauer, J.; Ugliengo, P.; Garrone, E.; Saunders, V. R. Theoretical Study of van der Waals Complexes at Surface Sites in Comparison with the Experiment. *Chem. Rev.* **1994**, *94*, 2095−2160.
(16) Van Santen, R. A.; Kramer, G. J. Reactivity Theory of Zeolitic Bronsted Acid Sites. *Chem. Rev.* **1995**, *95*, 637−660.
(17) Gounder, R.; Iglesia, E. The Roles of Entropy and Enthalpy in Stabilizing Ion-Pairs at Transition States in Zeolite Acid Catalysis. *Acc. Chem. Res.* **2012**, *45*, 229−235.
(18) Jones, A. J.; Iglesia, E. The Strength of Brønsted Acid Sites in Microporous Aluminosilicates. *ACS Catal.* **2015**, *5*, 5741−5755.
(19) Van Speybroeck, V.; Hemelsoet, K.; Joos, L.; Waroquier, M.; Bell, R. G.; Catlow, R. C. A. Advances in Theory and their Application within the field of Zeolite Chemistry. *Chem. Soc. Rev.* **2015**, *44*, 7044−7111.
(20) Boronat, M.; Corma, A. Factors Controlling the Acidity of Zeolites. *Catal. Lett.* **2015**, *145*, 162−172.
(21) Farneth, W. E.; Gorte, R. J. Methods for Characterizing Zeolite Acidity. *Chem. Rev.* **1995**, *95*, 615−635.
(22) Lercher, J. A.; Grundling, C.; EderMirth, G. Infrared Studies of the Surface Acidity of Oxides and Zeolites using Adsorbed Probe Molecules. *Catal. Today* **1996**, *27*, 353−376.
(23) Sato, H. Acidity Control and Catalysis of Pentasil Zeolites. *Catal. Rev.: Sci. Eng.* **1997**, *39*, 395−424.
(24) Garrone, E.; Otero-Arean, C. Variable Temperature Infrared Spectroscopy: A convenient Tool for Studying the Thermodynamics of Weak Solid−Gas Interactions. *Chem. Soc. Rev.* **2005**, *34*, 846−857.
(25) Busca, G. Acid Catalysts in Industrial Hydrocarbon Chemistry. *Chem. Rev.* **2007**, *107*, 5366−5410.
(26) Vimont, A.; Thibault-Starzyk, F.; Daturi, F.-M. Analysing and Understanding the Active Site by IR Spectroscopy. *Chem. Soc. Rev.* **2010**, *39*, 4928−4950.
(27) Derouane, E. G.; Vedrine, J. C.; Pinto, R. R.; Borges, P. M.; Costa, L.; Lemos, M. A. N. D. A.; Lemos, F.; Ribeiro, F. R. The Acidity of Zeolites: Concepts, Measurements and Relation to Catalysis: A Review on Experimental and Theoretical Methods for the Study of Zeolite Acidity. *Catal. Rev.: Sci. Eng.* **2013**, *55*, 454−515.
(28) Bordiga, S.; Lamberti, C.; Bonino, F.; Travert, A.; Thibault-Starzyk, F. Probing Zeolites by Vibrational Spectroscopies. *Chem. Soc. Rev.* **2015**, *44*, 7262−7341.
(29) Gorte, R. J.; White, D. Interactions of Chemical Species with Acid Sites in Zeolites. *Top. Catal.* **1997**, *4*, 57−69.
(30) Zheng, A.; Li, Sh.; Liu, S.-B.; Deng, F. Acidic Properties and Structure-Activity Correlations of Solid Acid Catalysts Revealed by Solid-State NMR Spectroscopy. *Acc. Chem. Res.* **2016**, *49*, 655−663.
(31) Brand, H. V.; Curtiss, L. A.; Iton, L. E. Computational Studies of Acid Sites in ZSM-5: Dependence on Cluster Size. *J. Phys. Chem.* **1992**, *96*, 7725−7732.
(32) Brand, H. V.; Curtiss, L. A.; Iton, L. E. Ab Initio Molecular Orbital Cluster Studies of the Zeolite ZSM-5. 1. Proton Affinities. *J. Phys. Chem.* **1993**, *97*, 12773−12782.
(33) Eichler, U.; Brändle, M.; Sauer, J. Predicting Absolute and Site Specific Acidities for Zeolite Catalysts by a Combined Quantum Mechanics/Interatomic Potential Function Approach. *J. Phys. Chem. B* **1997**, *101*, 10035−10050.
(34) Brändle, M.; Sauer, J. Acidity Differences between Inorganic Solids Induced by Their Framework Structure. A Combined Quantum Mechanics/Molecular Mechanics ab Initio Study on Zeolites. *J. Am. Chem. Soc.* **1998**, *120*, 1556−1570.
(35) Jones, A. J.; Carr, R. T.; Zones, S. I.; Iglesia, E. Acid Strength and Solvation in Catalysis by MFI Zeolites and Effects of the Identity, Concentration and Location of Framework Heteroatoms. *J. Catal.* **2014**, *312*, 58−68.
(36) Grajciar, L.; Arean, C. O.; Pulido, A.; Nachtigall, P. Periodic DFT investigation of the effect of aluminium content on the properties of the acid zeolite H-FER. *Phys. Chem. Chem. Phys.* **2010**, *12*, 1497−1506.
(37) Sauer, J.; Sierka, M. Combining Quantum Mechanics and Interatomic Potential Functions in Ab Initio Studies of Extended Systems. *J. Comput. Chem.* **2000**, *21*, 1470−1493.
(38) Lesthaeghe, D.; Van Speybroeck, V.; Waroquier, M. Theoretical Evaluation of Zeolite Confinement Effects on the Reactivity of bulky Intermediates. *Phys. Chem. Chem. Phys.* **2009**, *11*, 5222−5226.
(39) Gounder, R.; Iglesia, E. The Catalytic Diversity of Zeolites: Confinement and Solvation Effects within Voids of Molecular Dimensions. *Chem. Commun.* **2013**, *49*, 3491−3509.
(40) Derouane, E. G.; Andre, J. M.; Lucas, A. A. Surface Curvature Effects in Physisorption and Catalysis by Microporous Solids and Molecular Sieves. *J. Catal.* **1988**, *110*, 58−73.
(41) Derouane, E. G. Zeolites as Solid Solvents. *J. Mol. Catal. A: Chem.* **1998**, *134*, 29−45.
(42) Smit, B.; Maesen, T. L. M. Molecular Simulations of Zeolites: Adsorption, Diffusion, and Shape Selectivity. *Chem. Rev.* **2008**, *108*, 4125−4184.
(43) Klimes, J.; Michaelides, A. Perspective: Advances and Challenges in Treating van der Waals Dispersion Forces in Density Functional Theory. *J. Chem. Phys.* **2012**, *137*, 120901.
(44) Göltl, F.; Grüneis, A.; Bucko, T.; Hafner, J. Van der Waals Interactions Between Hydrocarbon Molecules and Zeolites: Periodic Calculations at Different Levels of Theory, from Density Functional Theory to the Random Phase Approximation and Møller-Plesset Perturbation Theory. *J. Chem. Phys.* **2012**, *137*, 114111.
(45) Gomes, J.; Zimmerman, P. M.; Head-Gordon, M.; Bell, A. T. Accurate Prediction of Hydrocarbon Interactions with Zeolites Utilizing Improved Exchange-Correlation Functionals and QM/MM Methods: Benchmark Calculations of Adsorption Enthalpies and Application to Ethene Methylation by Methanol. *J. Phys. Chem. C* **2012**, *116*, 15406−15414.
(46) Grimme, S. Accurate Description of van der Waals Complexes by Density Functional Theory Including Empirical Corrections. *J. Comput. Chem.* **2004**, *25*, 1463−1473.
(47) Grimme, S. Semiempirical GGA-Type Density Functional Constructed with a Long-Range Dispersion Correction. *J. Comput. Chem.* **2006**, *27*, 1787−1799.
(48) de Moor, B. A.; Reyniers, M. F.; Gobin, O. C.; Lercher, J. A.; Marin, G. B. Adsorption of C2-C8 n-Alkanes in Zeolites. *J. Phys. Chem. C* **2011**, *115*, 1204−1219.
(49) Wakabayashi, F.; Kondo, J.; Wada, A.; Domen; Hirose, C. FT-IR Studies of the Interaction between Zeolitic Hydroxyl Groups and Small Molecules. 1. Adsorption of Nitrogen on H-Mordenite at Low Temperature. *J. Phys. Chem.* **1993**, *97*, 10761−10768.
(50) Bordiga, S.; Regli, L.; Cocina, D.; Lamberti, C.; Bjorgen, M.; Lillerud, K. P. Assessing the Acidity of High Silica Chabazite H-SSZ-13 by FTIR Using CO as Molecular Probe: Comparison with H-SAPO-34. *J. Phys. Chem. B* **2005**, *109*, 2779−2784.
(51) Arean, C. O.; Delgado, M. R.; Nachtigall, P.; Thang, H. V.; Rubes, M.; Bulanek, R.; Chlubna-Eliasova, P. Measuring the Brønsted Acid Strength of Zeolites − does it Correlate with the O−H Frequency Shift probed by a weak Base? *Phys. Chem. Chem. Phys.* **2014**, *16*, 10129−10141.
(52) Boscoboinik, J. A.; Yu, X.; Yang, B.; Fischer, F. D.; Włodarczyk, R.; Sierka, M.; Shaikhutdinov, S.; Sauer, J.; Freund, H.-J. Modeling Zeolites with Metal-Supported Two-Dimensional Aluminosilicate Films. *Angew. Chem., Int. Ed.* **2012**, *51*, 6005−6008.

DOI: 10.1021/acscatal.8b04317
ACS Catal. 2019, 9, 1539−1548

(53) Boscoboinik, J. A.; Yu, X.; Emmez, E.; Yang, B.; Shaikhutdinov, Sh.; Fischer, F. D.; Sauer, J.; Freund, H.-J. Interaction of Probe Molecules with Bridging Hydroxyls of Two- Dimensional Zeolites: A Surface Science Approach. *J. Phys. Chem. C* **2013**, *117*, 13547−13556.
(54) Nachtigall, P.; Bludsky, O.; Grajciar, L.; Nachtigallova, D.; Delgado, M. R.; Arean, C. O. Computational and FTIR Spectroscopic Studies on Carbon Monoxide and Dinitrogen Adsorption on a High-Silica H-FER Zeolite. *Phys. Chem. Chem. Phys.* **2009**, *11*, 791−802.
(55) Gorte, R. J. What Do We Know About the Acidity of Solid Acids? *Catal. Lett.* **1999**, *62*, 1−13.
(56) Suzuki, K.; Noda, T.; Katada, N.; Niwa, M. IRMS-TPD of Ammonia: Direct and Individual Measurement of Brønsted Acidity in Zeolites and its Relationship with the Catalytic Cracking Activity. *J. Catal.* **2007**, *250*, 151−160.
(57) Niwa, M.; Katada, N. New Method for the Temperature-Programmed Desorption (TPD) of Ammonia Experiment for Characterization of Zeolite Acidity: A Review. *Chem. Rec.* **2013**, *13*, 432−4557.
(58) Parrillo, D. J.; Gorte, R. J.; Farneth, W. E. A Calorimetric Study of Simple Bases in H-ZSM-5: A Comparison with Gas-Phase and Solution-Phase Acidities. *J. Am. Chem. Soc.* **1993**, *115*, 12441−12445.
(59) Lee, C.; Parrillo, D. J.; Gorte, R. J.; Farneth, W. E. Relationship between Differential Heats of Adsorption and Brønsted Acid Strengths of Acidic Zeolites: H-ZSM-5 and H-Mordenite. *J. Am. Chem. Soc.* **1996**, *118*, 3262−32687.
(60) Perdew, J. P.; Burke, K.; Ernzerhof, M. Generalized Gradient Approximation Made Simple. *Phys. Rev. Lett.* **1996**, *77*, 3865−3868.
(61) Perdew, J. P.; Burke, K.; Ernzerhof, M. Generalized Gradient Approximation Made Simple. *Phys. Rev. Lett.* **1997**, *78*, 1396−1396.
(62) Kresse, G.; Furthmüller, J. Efficient Iterative Schemes for ab initio Total-Energy Calculations using a Plane-Wave Basis Set. *Phys. Rev. B: Condens. Matter Mater. Phys.* **1996**, *54*, 11169−11186.
(63) Blöchl, P. E. Projector Augmented Wave Method. *Phys. Rev. B: Condens. Matter Mater. Phys.* **1994**, *50*, 17953−17979.

DOI: 10.1021/acscatal.8b04317
ACS Catal. 2019, 9, 1539−1548